RSC Advances

PAPER

View Article Online
View Journal | View Issue

CrossMark click for updates

Cite this: *RSC Adv.*, 2017, **7**, 14888

Templated fabrication of pH-responsive poly(L-glutamic acid) based nanogels *via* surface-grafting and macromolecular crosslinking

Shifeng Yan,*[a] Yuanyuan Sun,[a] An Chen,[a] Lei Liu,[b] Kunxi Zhang,[a] Guifei Li,[a] Yourong Duan*[b] and Jingbo Yin*[a]

A novel class of pH-responsive hollow poly(L-glutamic acid)/chitosan (PLGA/CS) nanogels was fabricated by a templating approach, which was mild and surfactant free, and combined with a "grafting from" method and intermacromolecular crosslinking technique. The surface grafting, crosslinking reaction, nanogel fabrication and microstructure were investigated by FTIR, ^{1}H NMR, XRD, TGA, light scattering, and electron microscopy. The size of the resultant PLGA/CS nanogels could be accurately controlled by simply changing the size of the silica template. The nanogels responded to changes in environmental pH, elucidated according to the variation of the size of the nanogels and zeta potential at different pH values. Taking water-soluble antineoplastic agent mitoxantrone (MTX) as a model drug, the nanogels presented high loading ability at high-pH environment and rapid MTX release behavior under acidic conditions. MTT assays used to study the *in vitro* cytotoxicity of PLGA/CS nanogels showed a negligible cytotoxicity in mouse fibroblast L929 cells. Compared with bare MTX, MTX loaded PLGA/CS nanogels exhibited an enhanced inhibition effect to human gastric carcinoma SGC7901 cells. Fluorescence microscopy and flow cytometry analysis results demonstrated efficient cellular uptake of the PLGA/CS nanogels into the cells. These studies suggest that such pH-responsive PLGA/CS hollow nanogels might have great potential in controlled drug delivery systems.

Received 15th January 2017
Accepted 27th February 2017

DOI: 10.1039/c7ra00631d

rsc.li/rsc-advances

Open Access Article. Published on 07 March 2017. Downloaded on 2/2/2026 8:09:38 AM.
This article is licensed under a Creative Commons Attribution-NonCommercial 3.0 Unported Licence.

1. Introduction

Nanogels are nanometer sized hydrogel nanoparticles formed by physically or chemically cross-linked polymer networks. Nanogels are currently attracting significant attention and becoming a research target of great significance for their potential use in advanced technologies such as drug delivery systems and bioimaging.[1,2] As smart nanocarriers, they can trigger the release of bioactive agents, such as drugs, genes, and proteins, in response to specific cellular signals.

Various methods have been adopted to obtain nanogels. The commonly used emulsion polymerization shows the drawbacks of the use of organic solvents/surfactants, and the need of energy (*e.g.*, sonication) to form the emulsion, which may inactivate the entrapped therapeutic molecules. Also, the obtained nanogels are often strongly polydisperse in size.[3,4] For biomedical applications, the formation of nanogels with controllable size and polydispersity, while avoiding the use of solvents/surfactants is highly desirable and presents a challenge.[5]

Recently, the nano template methods have been developed and attracted great attention because they avoid the use of organic solvents/surfactants, and regulate the particle size using well-defined templates.[6] Hollow nanogels can be prepared using nanoparticles (*e.g.*, monodispersive gold[5] or silica[6] nanoparticles) as a sacrificial template, which are of particular interest because they also possess the ability to function as nanocapsules. Meanwhile, to prevent dissolution of the nanogel in the aqueous environment, chemical crosslinks involving the formation of covalent bonds are preferred to physical crosslinks.[7]

However, the major challenge of using nano template methods for nanogel preparation is colloidal stability. The versatile precipitation method proposed by Mohwald *et al.*[8] for the synthesis of hollow capsules was based on polymer precipitation onto the templates, which easily led to particle aggregation under poor solvent conditions for polymer shells.[6]

Moreover, the polymer materials employed for the encapsulation of the sacrificial nanosized template mainly focussed on non-degradable synthetic hydrophilic polymers, such as most commonly studied thermoresponsive poly(*N*-isopropylacrylamide),[5] pH-responsive polymethacrylic acid/polymethyl acrylate.[9] These non-degradable polymers, however, is typically regarded as not appropriate for many applications in drug delivery. Moreover, in the process of crosslinking of grafted or absorbed polymer chains

[a]*Department of Polymer Materials, Shanghai University, 333 Nanchen Road, Shanghai 200444, People's Republic of China. E-mail: yansf@staff.shu.edu.cn; jbyin@oa.shu.edu.cn*

[b]*Shanghai Cancer Institute, Renji Hospital, School of Medicine, Shanghai Jiao Tong University, Shanghai 200032, People's Republic of China. E-mail: yrduan@shsci.org*

This journal is © The Royal Society of Chemistry 2017

Open Access Article. Published on 07 March 2017. Downloaded on 2/2/2026 8:09:38 AM.
This article is licensed under a Creative Commons Attribution-NonCommercial 3.0 Unported Licence.

on the surface of nanosized template, some cytotoxic reagents, such as crosslinking agent, initiator, and monomer are often used, which are the major obstacles in the use of drug carriers.

Thus, there still exists a need to develop a nano template method for yielding biodegradable and biocompatible hollow nanogels with good control over the properties and dimensions in the nanometer range.

Poly(L-glutamic acid) (PLGA) is a synthetic polypeptide that can biodegrade into naturally occurring glutamic acid. The pendent-free carboxyl groups in each repeating unit make it responsive to external stimuli (such as pH and electrolytes), and provide functionality for drug attachment. These features make PLGA a promising candidate for application in the drug delivery. The pH-responsive PLGA based nanogels are of special interest in the delivery of anti-cancer drugs due to the acidic extracellular pH environment of solid tumors and the numerous pH gradients that exist in the body.[10,11] However, few reports showed that PLGA served as a nanogel in drug delivery systems.

In this report, we described a strategy for synthesizing hollow PLGA based nanogels using SiO_2 as the sacrificed template. We have combined the templating approach with a "grafting from" method and intermacromolecules crosslinking technique. The synthetic route toward the formation of hollow PLGA based nanogels involved the surface-initiated ring-opening polymerization (ROP) of γ-benzyl-L-glutamate *N*-carboxyanhydride (BLG-NCA) and grafting of PLGA onto SiO_2 nanoparticles, then crosslinking of PLGA using chitosan (CS) as macromolecular crosslinking agent, followed by dissolution of the SiO_2 core as depicted in Scheme 1.

This work provided a complementary methodology for the synthesis of hollow polypeptide based nanogels. Advantages of the method include: (1) "grafting from" method enabling high grafting density of polypeptides and well-dispersion of SiO_2 templates, (2) preparation of hollow nanogels based on only water-soluble biodegradable materials (synthetic polypeptides and nature polymers) without using organic solvents and surfactants, (3) fabrication of hollow nanogels from stable covalently cross-linked networks using macromolecular crosslinking agent without introduction of toxic small molecule crosslinking agent, initiator, and monomer, (4) easy control over the nanogel dimensions and wall thickness, (5) expected pH-dependent behavior of nanogels considering the component polymers were both weak polyelectrolytes.

The surface grafting of PLGA onto template nanoparticles, and fabrication of PLGA/CS nanogels were described. Various physicochemical characteristics including micromorphology, hollow structure, particle size, surface charge, pH responsiveness, drug loading and release were investigated. Biological investigations including cytotoxicity evaluation and cellular uptake cytotoxicity assays were performed.

2. Experimental

2.1. Materials

γ-Benzyl-L-glutamate (BLG) was purchased from Jier Biochemical Company and used without any further purification. BLG-NCA was synthesized as our previous work with slight modification.[12] Trimethylsilyl iodide (C_3H_9SiI), trifluoroacetic acid (TFA) and 3-aminopropyltriethoxysilane (APTS) were purchased from Aladdin Reagent Company (Shanghai). Tetraethyl orthosilicate (TEOS), ethanol (EtOH), ammonium hydroxide ($NH_3 \cdot H_2O$, 25–28%), hydrofluoric acid (HF, 40%), 1,4-dioxane and dichloromethane (CH_2Cl_2) were purchased from Shanghai Chemical Reagent Co., Ltd. 1,4-Dioxane and dichloromethane were further distilled before use. Chitosan (CS) ($M_v = 4.0 \times 10^4$) was purchased from Jinan Haidebei Marine Bioengineering Corp. (Shandong, China). 1-Ethyl-3-(3-dimethylaminopropyl) carbodiimide hydrochloride (EDC) and 1-hydroxypyrrolidine-2,5-dione (NHS) were purchased from Covalent Chemical Technology Co., Ltd. (Shanghai, China). Mitoxantrone (MTX) was purchased from Beijing Shilian Hengtong Chemical Technology Co., Ltd. (Beijing, China).

Methyl thiazolyl tetrazolium (MTT), rhodamine B (RB), paraformaldehyde (PFA) and dihydrochloride 2-(4amidinophenyl)-6-indolecarbamidine (DAPI) were obtained from the Sigma-Aldrich Co., Ltd. The common mouse fibroblast L929 cells and

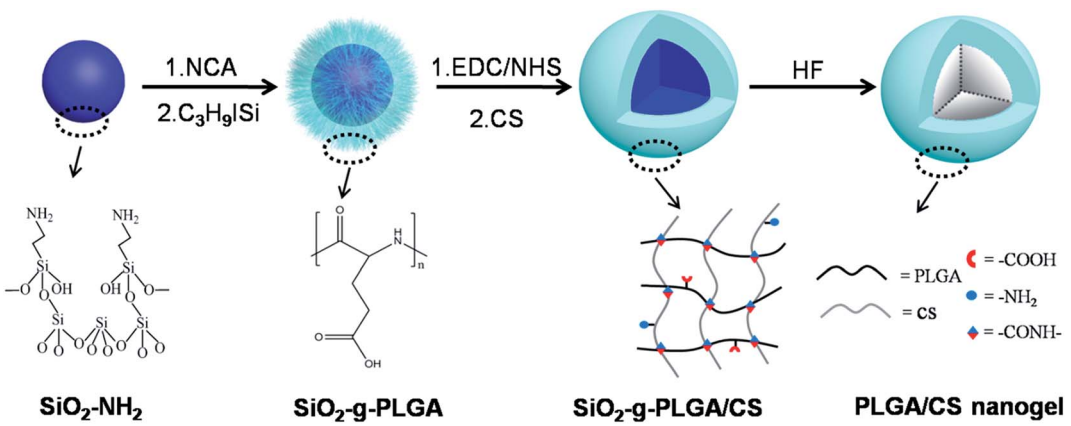

Scheme 1 Schematic illustration for the preparation of PLGA/CS nanogels. The synthetic route involves the surface-initiated grafting of PLGA onto SiO_2 nanoparticles, then crosslinking of PLGA using chitosan as macromolecular crosslinking agent, followed by dissolution of the SiO_2 template.

Open Access Article. Published on 07 March 2017. Downloaded on 2/2/2026 8:09:38 AM. This article is licensed under a Creative Commons Attribution-NonCommercial 3.0 Unported Licence.

the human gastric carcinoma SGC7901 cells were obtained from the Shanghai Cancer Institute were grown in DMEM medium (Paisley, UK) containing 10% fetal bovine serum (FBS) at 37 °C in a humidified environment containing 5% CO_2.

2.2. Preparation of SiO_2-*g*-PLGA nanoparticles

2.2.1. Synthesis and surface amination of SiO_2 nanoparticles. The preparation of SiO_2 nanoparticles was performed according to Stöber synthesis.[13] Typically, a solution containing 6 mL of TEOS and 54 mL of EtOH were slowly added into a mixture solution containing 8–12 mL of $NH_3 \cdot H_2O$ and 148 mL of EtOH in 6 hours, and the reaction was continued for another 2 h. Then the resultant white SiO_2 precipitate nanoparticles were separated by centrifugation and then washed with ethanol and dried overnight under vacuum at 40 °C.

SiO_2 nanoparticles were then functionalized with a layer of primary amine groups by APTS grafting. In this process, SiO_2 nanoparticles (1.2 g) were dispersed in 184 mL of anhydrous ethanol. The dispersion was sonicated for 20 min before APTS was added. The mixture was refluxed at 85 °C for 6–8 h and followed by centrifugation, washing with ethanol for several times, and drying overnight under vacuum at 40 °C for 12 h. The obtained amino-functionalized SiO_2 nanoparticles were denoted as SiO_2–NH_2.

2.2.2. Surface grafting of PLGA onto SiO_2 nanoparticles. Using SiO_2–NH_2 as initiator, the surface grafting of poly(γ-benzyl-L-glutamate) (PBLG) was performed by the ring-opening polymerization of the *N*-carboxyanhydride of γ-benzyl-L-glutamate (BLG-NCA). 1 g of SiO_2–NH_2 powders were dispersed in 40 mL of dry 1,4-dioxane. The suspension was sonicated for about 2 h. Then a solution of 7 g of BLG-NCA in 100 mL of dry 1,4-dioxane was added. The mixture was allowed to stir for 3 days at 25 °C under a nitrogen atmosphere. After being precipitated into excess diethyl ether/ethanol (2/1, v/v) mixture, the obtained SiO_2-*g*-PBLG composite particles were further washed twice with diethyl ether and vacuum dried at room temperature for 24 h.

To remove the γ-benzyl protection groups and obtain the SiO_2-*g*-PLGA composite particles, the so-called "deprotection" step was accomplished by dissolving the SiO_2-*g*-PBLG (1 g) in dry CH_2Cl_2 (20 mL) followed by addition of excess C_3H_9SiI (0.4 mL). The resulting pale yellow solution was stirred under nitrogen at 40 °C for 24 h in dark. The SiO_2-*g*-PLGA was isolated by addition of a mixture solution containing EtOH, water and petroleum ether (with volume ratio 1 : 1 : 8), followed by filtration, washing with the mixture solution for several times, and drying overnight under vacuum at room temperature for 24 h.

2.3. Fabrication of PLGA/CS nanogels

To synthesize PLGA/CS nanogels, SiO_2-*g*-PLGA nanoparticles were dissolved in distilled water to obtain a 3 mg mL^{-1} solution. The pH of the solution was adjusted to 7 by the addition of 0.1 M HCl or NaOH solution. Then, EDC and NHS were added for activation of the carboxyl groups of SiO_2-*g*-PLGA. The molar ratio of NHS to EDC was set at 1 : 5, while –COOH of PLGA to EDC was 1 : 1, 2 : 1, 3 : 1, 4 : 1 and 5 : 1, respectively. A turbid solution was obtained after the dropwise addition of activated SiO_2-*g*-PLGA to an aqueous solution of CS (5 mg mL^{-1}, pH = 4.4). The molar ratio of –COOH of SiO_2-*g*-PLGA to –NH_2 of CS was set at 1 : 3. The reaction was allowed to proceed at room temperature for 12 h. Excess CS was removed by 2 cycles of centrifugation (13 000 rpm, 20 min) and washing with acetic acid solution (0.05 M, pH = 5.5).

Hollow PLGA/CS nanogels were obtained by dissolving the SiO_2 core of SiO_2-*g*-PLGA/CS composite nanoparticles in 4 mL of HF (5 M) aqueous solution for 2 h. After several cycles of centrifugation (13 000 rpm, 20 min) and washing with deionized water, the sedimentation of the PLGA/CS nanogel obtained was redispersed into deionized water or lyophilized for further use.

2.4. Physicochemical characterization

The FTIR spectra were recorded using a FT-IR spectrophotometer (AVATAR 370, Nicolet, USA) in the region of 4000–500 cm^{-1}.

The ^1H NMR spectra were obtained by an AV 500 NMR from BRUKER. Deuterated water (D_2O) was used as solvent for all the samples.

X-ray diffraction (XRD) patterns were analyzed using a diffractometer (D/MAX2550, Rigaku) with Cu Kα radiation at a voltage of 40 kV and 40 mA. The samples were scanned between 2θ = 5–60° with a scanning speed of 4° min^{-1}.

The thermal gravimetric analysis was examined by means of thermogravimetry with a heating rate of 10 °C min^{-1} in nitrogen atmosphere on TA Q-500 instruments.

To determine the molecular weight of PLGA chains, SiO_2-*g*-PLGA was dissolved in TFA. Then HF aqueous solution was added to etch SiO_2 cores. After 2 hours, PLGA was precipitated by abundant EtOH. The fibrous polymer was washed with EtOH/water (1 : 1, v/v) solution, isolated and vacuum dried. The viscosity-average molecular weight (M_v) was determined using an HH-W600 Ubbelohde viscometer (Ningbo Tianheng, China). The capillary diameter of the viscometer was 0.38 mm, and the experiment was performed in 0.4 M NaCl/0.01 M NaH_2PO_4 buffer solution (pH 7.05) at 25 °C. M_v was obtained from the Mark–Houwink equation: intrinsic viscosity $[\eta] = K_m M_v^{\alpha}$, where $K_m = 2.93 \times 10^5$, and $\alpha = 0.923$.[14,15]

Zeta potentials were determined with Malvern Zetasizer 3000HS equipped with MPT-1 titrator (Malvern, Worcestershire, UK) at 25 °C. Electrophoretic mobilities were converted to zeta potentials using Smoluchowski's equation.

The morphology of PLGA/CS nanogel was observed by scanning electron microscopy (SEM, JEOL, JSM-6700F) and transmission electron microscopy (TEM, FEI, Tecnai G220 TWIN). Samples for SEM observation were prepared by depositing suspensions of nanogels on Si slides. The samples for TEM observation were dripped onto nitrocellulose-covered copper grids at room temperature.

The mean hydrodynamic particle diameter and particle size distribution (polydispersity index, PDI) in aqueous media were determined at λ = 632.8 nm and a scattering angle of 90° based on the cumulant method using an ALV/CGS-3 apparatus equipped with a 22 mW He–Ne laser as the light source. The angular dependence of the autocorrelation functions was measured

 This journal is © The Royal Society of Chemistry 2017

Open Access Article. Published on 07 March 2017. Downloaded on 2/2/2026 8:09:38 AM.
This article is licensed under a Creative Commons Attribution-NonCommercial 3.0 Unported Licence.

using the same instrument as described above. Correlation functions were also analyzed by the cumulant method at varying angles. To assess the geometrical morphology of the PLGA/CS nanogel, the mean hydrodynamic radius (R_h) was obtained at a scattering angle of 90° based on the CONTIN method. The root-mean-square radius of gyration (R_g) was evaluated by the angular dependent measurements of the light scattering intensity. A Zimm plot of the scattering intensity ($KC/R_{vv}(q)$, $R_{vv}(q)$ is known as the Rayleigh ratio) *versus* the square of the scattering vector (q^2) was used to determine R_g.[16]

UV-vis spectra were recorded on an Agilent 8453 UV-vis spectrophotometer.

2.5. Drug loading and release

In order to study the effect of pH value on the loading capacity of nanogels, 1 mg of the nanogels were incubated in 5 mL of mitoxantrone (MTX, 0.4 mg mL^{-1}) aqueous solution at different pH values (4, 5, 6, 7.4 and 9.5). After being incubated under various conditions for 1 h, the MTX-loaded nanogels were centrifuged (13 000 rpm, 20 min), washed for 2 times with deionized water and lyophilized for further use in release experiments. The concentration of MTX remained in the supernatant after centrifugation was measured at 609 nm wavelength, which was the UV-vis spectroscopy characteristic absorption wavelength. The MTX loading inside the nanogels was calculated from the change of MTX concentrations in the supernatant. All the data were averaged from 3 parallel experiments.

For the examination of MTX release, 5 mg of MTX-loaded nanogels were carefully enveloped into dialysis bags and exposed to 100 mL of buffer solution at different pH values of 4, 5, 6 and 7.4, respectively. Five milliliters buffer solution was fetched from release system with reconstitution of 5 mL fresh buffer solution at every predetermined time. The concentration of the MTX released from this drug delivery system was monitored at 609 nm of UV absorbance.

2.6. Cytotoxicity evaluation of PLGA/CS nanogels and antitumor activity of MTX-loaded PLGA/CS nanogels

The cytotoxicity of PLGA/CS nanogels was evaluated using the MTT assay in the common mouse fibroblast L929 cells. Briefly, the cells (5×10^3 per well) were seeded in 96-well plates and incubated for 24 h. Then PLGA/CS nanogels were added into each well at different concentrations ranging from 5 to 400 μg mL^{-1}. After 24 h and 48 h of incubation, 100 μL of stock solution of MTT was added to each well, and the cells were further incubated for 4 h at 37 °C. The culture medium was then removed from each well and replaced with 150 μL of DMSO. The absorbance was measured at 490 nm using a microplate reader (Bio-RAD, model 550). Untreated cells were taken as control with 100% viability.

The antitumor activity of MTX-loaded PLGA/CS nanogels was evaluated by MTT method. Human gastric carcinoma SGC7901 cells (5×10^3 per well) were cultured on a 96-well plates, and then incubated for 24 h. Then, the MTX and MTX-loaded nanogels were added to the wells at the MTX concentration of 0.1, 0.25, 0.5, 1.0, 1.5, 2.0, 3.0, 4.0 μg mL^{-1}, and the cells were incubated for an additional 24 h and 48 h. 100 μL of MTT solution (0.5 mg mL^{-1}) was added to each well, and the cells were further incubated for 4 h at 37 °C. The culture medium was then removed from each well and replaced with 150 μL of DMSO. The absorbance was measured at 490 nm using a microplate reader (Bio-RAD, model 550). Untreated cells were taken as control with 100% viability.

The inhibitory rate of SGC7901 cells was calculated according to following equation:

$$\text{Inhibitory rate} = \frac{A_{\text{control}} - A_{\text{drug}}}{A_{\text{control}}} \times 100\%$$

where A_{control} was the absorbance at the wavelength of 490 nm in the control groups, and A_{drug} was the absorbance in the MTX-loaded PLGA/CS nanogels groups.

The experimental data were expressed as means ± standard deviation (SD). Single factor analysis for variance (ANOVA) was used to assess the statistical significance of the results. Statistical significance was set to a p value ≤ 0.05.

2.7. Cellular uptake of fluorescent PLGA/CS nanogels

Rhodamine B (RB) was used as a fluorescence probe to facilitate the observation of cellular uptake of the PLGA/CS nanogels. Free RB was removed from the RB-loaded PLGA/CS nanogels by ultrafiltration. Human gastric carcinoma SGC7901 cells (5×10^4 per well) were seeded in 24-well plates and incubated for 24 h. The RB and RB-loaded nanogels were added to the wells at the RB concentration of 10, 50 and 100 μg mL^{-1}, and the cells were incubated for an additional 4 h. After removing the supernatant, the cells were fixed with 4% paraformaldehyde for 20 min and then 10 μg mL^{-1} 4,6-diamidino-2-phenylindole dihydrochloride (DAPI) was added for 10 min incubation. Subsequently, the cells were washed with PBS and sealed with glycerine. The cellular uptake was observed using the Olympus IX-51 fluorescence microscopy from Olympus Optical Company, Ltd (Tokyo, Japan).

2.8. Flow cytometer analysis of PLGA/CS nanogels

SGC7901 cells (2×10^5 per well) were seeded in 6-well plates and incubated for 24 h. The RB and RB-loaded nanogels were added to the wells at RB concentration of 50 μg mL^{-1}. After incubating for 4 h, the cells were then washed with PBS, trypsinized, harvested and resuspended in PBS. The cellular binding of the PLGA/CS nanogels was measured using a Sorp Fascaria II flow cytometer (Becton Dickinson, USA).

3. Result and discussion

3.1. Synthesis of SiO_2-*g*-PLGA nanoparticles

3.1.1. Template synthesis and surface amination. SiO_2 template nanoparticles were fabricated by Stöber method, which generally proceeds with the ammonia-catalyzed reaction of TEOS with water in low molecular weight alcohols and is known to obtain monodisperse spherical silica nanoparticles.[13,17] As shown in Fig. 1a, monodisperse SiO_2 nanoparticles with tunable and uniform size were fabricated. The

Open Access Article. Published on 07 March 2017. Downloaded on 2/2/2026 8:09:38 AM.
This article is licensed under a Creative Commons Attribution-NonCommercial 3.0 Unported Licence.

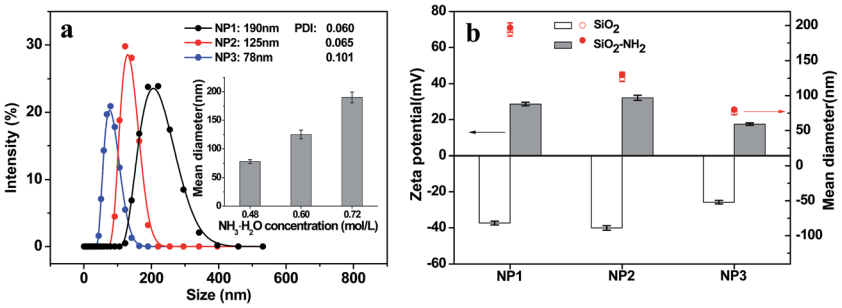

Fig. 1 Preparation and amination modification of SiO_2 templates. (a) Hydrodynamic diameter distribution of SiO_2 nanoparticles. Inset: SiO_2 size as a function of $NH_3 \cdot H_2O$ concentration. The SiO_2 nanoparticles with mean diameters of 190 nm, 125 nm, 76 nm were named as NP1, NP2 and NP3, respectively. (b) The zeta potential and size before and after amination modification of SiO_2 nanoparticles (NP1, NP2 and NP3).

SiO_2 nanoparticles with mean diameters of 190 nm, 125 nm, 76 nm were named as NP1, NP2 and NP3, respectively. The polydispersity index (PDI) of particle size was less than or equal to 0.1, illustrating good monodispersity of silica nanoparticles. Acting as a catalyst, the $NH_3 \cdot H_2O$ amount had a great effect on silica particle size. The mean diameters of SiO_2 nanoparticles increased rapidly from 76 to 190 nm, with the increase of $NH_3 \cdot H_2O$ concentration from 0.48 to 0.72 mol L^{-1}, as shown in the inset of Fig. 1a.

The zeta potential and size of SiO_2 nanoparticles before and after surface amination were displayed in Fig. 1b. As the existence of silanol groups on the surface, NP1, NP2 and NP3 showed the negative zeta potentials of −37.4, −40.1 and −25.8 mV, respectively. After amination, the zeta potentials changed to positive value of 28.7, 32.1 and 17.5 mV. Meanwhile, a slight increase in size was observed. All these findings indicated successful surface functionalization of SiO_2 nanoparticles with amino groups.

3.1.2. Grafting of PLGA onto template nanoparticles. The covalent grafting of polypeptides onto a silica nanoparticle is typically carried out *via* a "grafting-to" or "grafting-from" methodology. The "grafting to" approach presents a limitation of low grafting ratio, because the previously tethered polypeptides would block the surrounding linkage groups, thus hindering subsequent attachment and further reaction.[18] While for "grafting from" method, it is more likely to achieve high grafting density. The chemical synthetic route applied in our "grafting from" approach was conducted through ROP of BLG-NCA initiated by free primary amino groups on the surface of SiO_2–NH_2 nanoparticles.[19,20] Although it has been reported that the silica particles with the shell of poly(carbobenzoxy-L-lysine) and poly(benzyl-L-glutamate) were fabricated by surface initiated ring-opening polymerization of *N*-carboxyanhydride (NCA) monomers,[21] the deprotection remains a challenge. Some harsh reaction conditions ($HBr/Cl_2CHCOOH$, base) inevitably affects the stability of silica core, length of the polymer chain, and covalent linkage between silica core and the polypeptide shell. In our study, a mild deprotection reagent Me_3SiI,[20] was used to remove the benzyl groups from BLG units and obtain the silica-PLGA core–shell nanoparticles. The strategy was outlined in Fig. 2a.

Surface grafting of PLGA was confirmed by FTIR, XRD, and ^1H NMR spectra. Fig. 2b demonstrated FTIR spectra of SiO_2 before and after surface modification. The SiO_2 nanoparticles showed the characteristic bands at about 1063, 805 and 1633 cm^{-1}, which were ascribed to Si–O–Si, O–Si–O and Si–OH bands, respectively.[22] Compared with SiO_2, SiO_2–NH_2 nanoparticles exhibited a broader peak at 3425 cm^{-1}, corresponding to the co-existence of both –OH and –NH_2 groups. Surface grafting of poly(γ-benzyl-L-glutamate) onto SiO_2 nanoparticles was monitored by observation of new peaks of ν(C=O) at 1739 cm^{-1}, amide I and II at 1652 and 1546 cm^{-1}, $\nu(C_{sp^2}–H$ of benzene ring) at 3050 cm^{-1}. For SiO_2-*g*-PLGA, the peak at 3050 cm^{-1} disappeared, indicating successful deprotection of the benzyl group. Meanwhile, the peak at 1739 cm^{-1} shifted to 1727 cm^{-1} and became broader, indicating the appearance of carboxy groups.[23]

The representative ^1H NMR spectra of SiO_2-*g*-PLGA with different core size of SiO_2 nanoparticles were presented in Fig. 2c. The alphabetically labeled peaks were assigned to the corresponding protons shown in inset scheme. The peaks at 1.78, 1.88, 2.11 and 4.16 ppm were characteristic of proton peaks of PLGA, which was in accordance with previous result.[24]

Bare SiO_2 nanoparticles precipitated rapidly in water. The grafted PLGA played an important role in the dispersion of SiO_2 nanoparticles. It could be obviously seen from Fig. 2d that the SiO_2-*g*-PLGA nanoparticles were soluble in water. The solutions were stable for more than 1 month without any precipitation. The excellent solubility of SiO_2-*g*-PLGA nanoparticles also confirmed the existence of grafted PLGA shell, and would be beneficial for further preparation of PLGA/CS nanogels.

The comparison of typical XRD patterns of SiO_2 before and after surface grafting of PLGA was displayed in Fig. 2e. For SiO_2 nanoparticles, a broad peak centered at 22.3° was observed, corresponding to the characteristic diffraction of amorphous silica. The diffractogram of PLGA consisted of two weak crystallization peaks at $2\theta = 8.1°$ and 19.8°,[23] due to its low crystallizability. For SiO_2-*g*-PLGA nanoparticles, the peak at $2\theta = 8.1°$ was still observed, and a broad peak over the range of 15–35° was detected, ascribing to the overlap of the peaks for both PLGA and SiO_2. This indicated the PLGA was grafted onto SiO_2 nanoparticles, and the surface grafting did not destruct the original crystalline structure of PLGA.

To determine the molecular weight of grafted PLGA chains, the grafted PLGA was collected and measured after dissolving the silica core. As shown in Fig. 2f, all of the SiO_2-*g*-PLGA

 This journal is © The Royal Society of Chemistry 2017

Open Access Article. Published on 07 March 2017. Downloaded on 2/2/2026 8:09:38 AM.
This article is licensed under a Creative Commons Attribution-NonCommercial 3.0 Unported Licence.

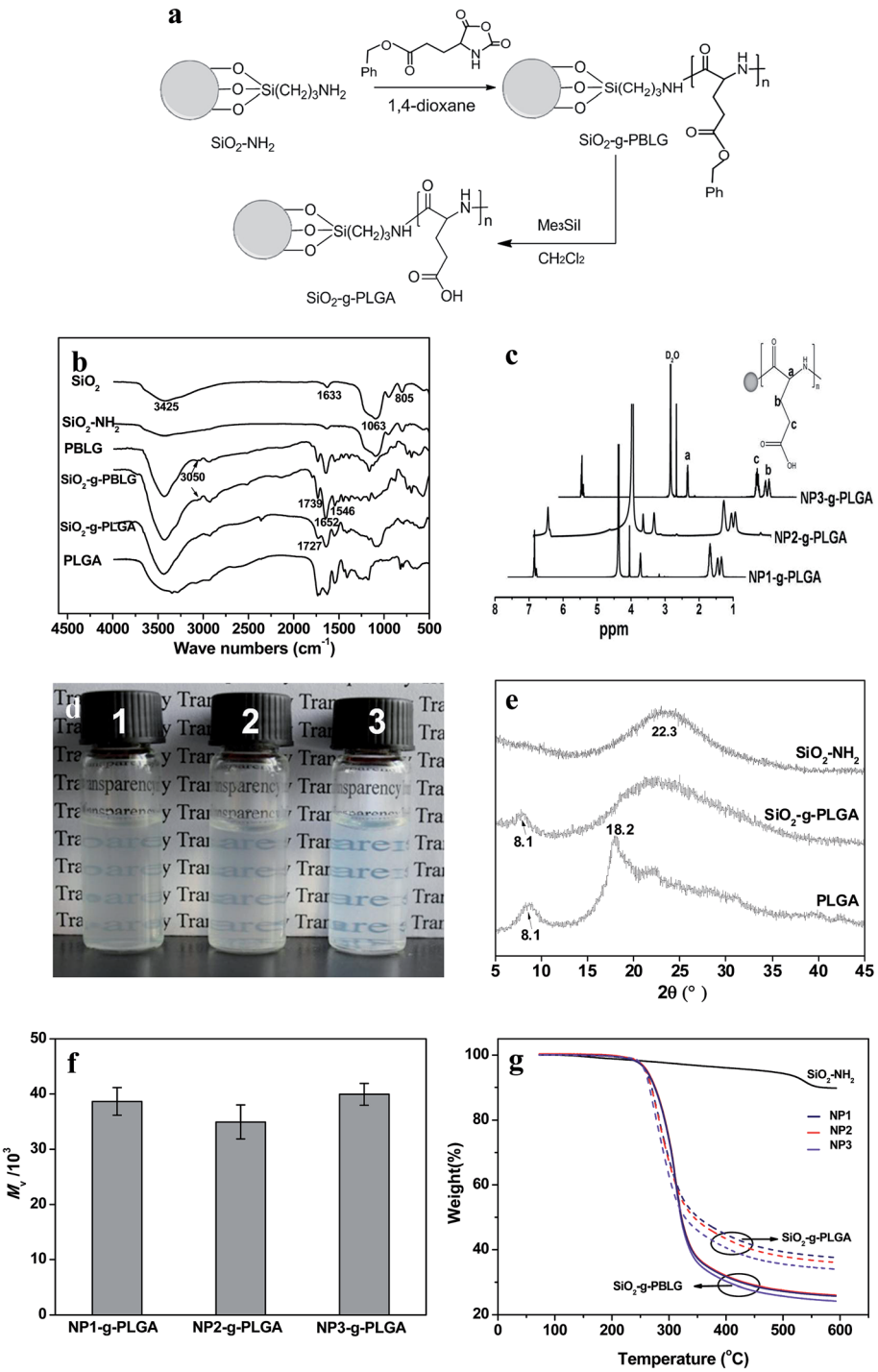

Fig. 2 Synthesis of SiO_2-*g*-PLGA composite nanoparticles. (a) Schematic illustration for surface grating of PLGA onto SiO_2 nanoparticles. (b) FTIR spectra of SiO_2, SiO_2–NH_2, PBLG, SiO_2-*g*-PBLG, SiO_2-*g*-PLGA and PLGA. (c) ^{1}H NMR spectra of various SiO_2-*g*-PLGA (NP1-*g*-PLGA, NP2-*g*-PLGA and NP3-*g*-PLGA) composite nanoparticles. (d) Digital photographs of various SiO_2-*g*-PLGA aqueous solutions with a concentration of 0.3 wt%. (e) X-ray diffraction patterns of SiO_2–NH_2, SiO_2-*g*-PLGA and PLGA. (f) Viscosity-average molecular of grafted PLGA for various SiO_2-*g*-PLGA composite nanoparticles. (g) TGA curves of SiO_2-*g*-PBLG (solid line) and SiO_2-*g*-PLGA (dash line).

nanoparticles (NP1, NP2 and NP3) exhibited similar viscosity-average molecular weight (M_v) of grafted PLGA with the value of about 4×10^4.

The grafted amount of PBLG and PLGA was estimated by TGA.[25] Before heated to 600 °C, all samples were heated to 120 °C to eliminate water or solvent, so the weight loss of composite particles minus that of SiO_2–NH_2 could be approximately the amount of grafted PBLG or PLGA.[26] As shown in Fig. 2g, SiO_2–NH_2 and NP1-*g*-PBLG, NP2-*g*-PBLG and NP3-*g*-PBLG showed weight loss of 10.7, 74.3, 73.5 and 70.5 wt%,

Open Access Article. Published on 07 March 2017. Downloaded on 2/2/2026 8:09:38 AM.
This article is licensed under a Creative Commons Attribution-NonCommercial 3.0 Unported Licence.

respectively. After deprotection of the benzyl group, SiO_2-*g*-PLGA showed the corresponding weight loss of 66, 65.7 and 63.4 wt%. Therefore, the grafted amount of PLGA was in the range of 52–55%, the values of which were very similar for NP1, NP2 and NP3.

3.2. Fabrication of PLGA/CS nanogels

To prepare the PLGA/CS nanogels, PLGA shell of SiO_2-*g*-PLGA nanoparticles was crosslinked using chitosan (CS) as macromolecular, followed by dissolution of the SiO_2 core. PLGA/CS complexation between PLGA and CS in the form of porous scaffolds[27] and porous microspheres[28] has been scrutinized in our previous work. However, the stable PLGA/CS nanogels based on electrostatic interaction could not be obtained because of the dissolution and collapse of the PLGA/CS polyelectrolyte complex shell during removal of silica core in HF solution. Thus, the chemical crosslinking between SiO_2-*g*-PLGA and CS was highly desirable.

EDC and NHS were used as the carboxylic acid activators, which were non-toxic and could realize "zero length" amide crosslinks between carboxyl groups from SiO_2-*g*-PLGA and amino groups from CS.[29,30] As presented in Fig. 3a, EDC was used as a dehydrating agent to activate carboxyl groups to a reactive *O*-acylisourea, followed by formation of a semi-stable NHS ester. Aminolysis of NHS ester with amino groups of CS resulted in a stable network structure crosslinked by amide bonds.

The EDC amount had a great effect on stability of the resulting PLGA/CS nanogels. Stable PLGA/CS nanogels could only be obtained when EDC/–COOH molar ratio was not less than 3 : 1. Less amount of EDC led to the collapse of the hydrogel and precipitate of PLGA during removal of silica core in HF solution, which might be ascribed to low activation efficiency and crosslinking density between PLGA and CS.

Three kinds of nanogels named NG1, NG2 and NG3 were fabricated using SiO_2-*g*-PLGA with the silica core of NP1, NP2 and NP3 as precursors. The molar ratio of EDC to –COOH was set at 5 : 1.

The procedure in the fabrication of nanogels was followed by microelectrophoresis, as shown in Fig. 3b. SiO_2-*g*-PLGA possessed negative charge with the zeta potential ranging from −62 to −78 mV because some carboxylate groups ionized in aqueous solution, while CS with NH_3^+ was positive charged with the zeta potential of 79 mV. Compared with SiO_2-*g*-PLGA, the PLGA/CS nanogels decreased drastically in zeta potential, confirming the consumption of carboxyl groups from grafted PLGA and the introduction of amino groups from CS.

The FTIR spectra were displayed in Fig. 3c. For SiO_2-*g*-PLGA, the absorption bands located at 1727, 1627 and 1538 cm^{-1} originated from C=O, amide I and II groups of PLGA, while the absorption band at 1063 cm^{-1} was attributed to the Si–O–Si stretching vibration.[22] With respect to CS, the characteristic absorption band at 3429 cm^{-1} was attributed to the stretching vibration of the N–H group bonded to the O–H group, the peaks at 1657 cm^{-1} were ascribed to amide groups,[31] and the peak at 1101 cm^{-1} was attributed to vibrational modes of the saccharide units.[32] As for SiO_2-*g*-PLGA/CS nanogels, the original characteristic absorption bands of C=O group at 1727 cm^{-1} and

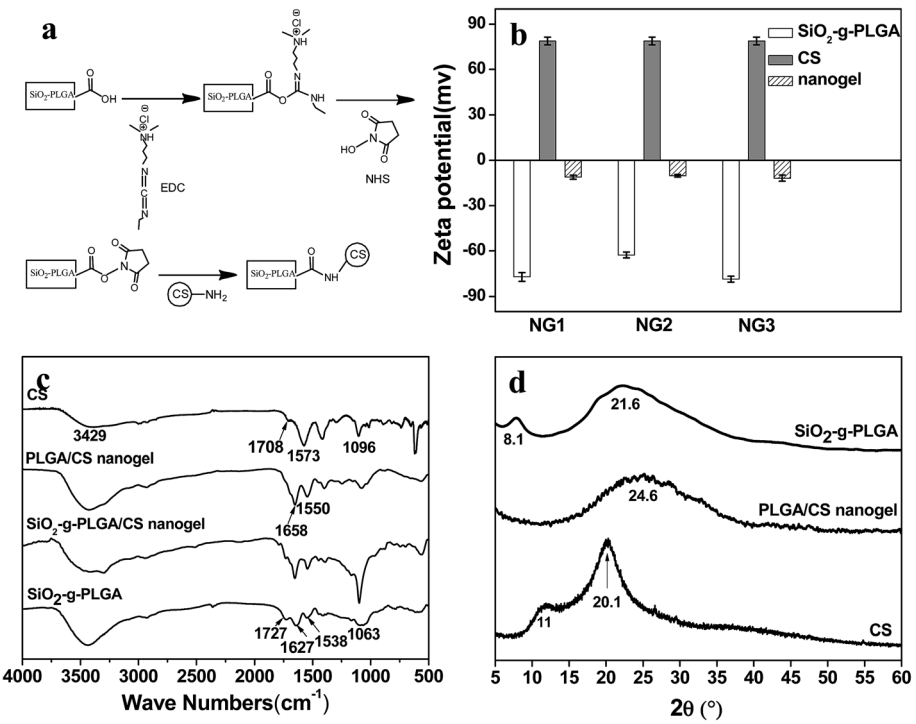

Fig. 3 Fabrication of PLGA/CS nanogels. (a) Schematic presentation of activation behaviors of SiO_2-*g*-PLGA and chemical crosslinking with CS. (b) The change in zeta potential during the preparation process. (c) FTIR spectra and (d) X-ray diffraction patterns of CS, SiO_2-*g*-PLGA, SiO_2-*g*-PLGA/CS and PLGA/CS nanogel.

 This journal is © The Royal Society of Chemistry 2017

Open Access Article. Published on 07 March 2017. Downloaded on 2/2/2026 8:09:38 AM.
This article is licensed under a Creative Commons Attribution-NonCommercial 3.0 Unported Licence.

amide II group at 1538 cm^{-1} for PLGA almost disappeared, also did those of amide bands for CS. New absorption bands appeared at peaks of 1658 and 1550 cm^{-1}, revealing chemical cross-linking between PLGA and CS. After core removal, the intensity of the silica's characteristic absorption band at 1063 cm^{-1} decreased greatly in the spectrum of PLGA/CS nanogels. Considering the existence of adjacent peak at 1101 cm^{-1} for CS, the weak absorption centered at 1063 cm^{-1} could be ascribed to trace residual silica.

XRD diffractogram was used to investigate the crystalline properties of CS, SiO_2-*g*-PLGA and PLGA/CS nanogels, as shown in Fig. 3d. The diffractogram of CS consisted of two major crystalline peaks at 11 and 20.1°, indicating a certain degree of crystallinity. SiO_2-*g*-PLGA exhibited weak peaks at around 8.1 and 21.6°, due to its low crystallizability. However, for the PLGA/CS nanogels, only a broad peak centered at 24.6° was detected. This indicated that the cross-linking between SiO_2-*g*-PLGA and CS resulted in destruction of the original crystalline structure of component polymers.

3.3. Micromorphology and microstructure of PLGA/CS nanogels

3.3.1. Micromorphology of PLGA/CS nanogels. SEM and TEM observations were conducted to follow the surface grafting of PLGA onto SiO_2 nanoparticles and examine the micromorphology of PLGA/CS nanogels before and after core removal, as displayed in Fig. 4.

The spherical, uncoated SiO_2 nanoparticles (NP1) were dispersed with a slight agglomeration (Fig. 4a). The average diameter was about 190 nm, in accordance with the result in Fig. 1a. The diameter of SiO_2 nanoparticles increased to 230 nm after PLGA surface grafting (Fig. 4b). After crosslinking with CS, the SiO_2-*g*-PLGA/CS nanogels showed a much larger diameter of 295 nm (Fig. 4c). After core removal, PLGA/CS nanogels retained the original shape with no sign of rupture or collapse, but the size of which (*ca.* 100 nm) was much smaller than that of SiO_2-*g*-PLGA/CS nanogels. We believed that during the drying process, hollow nanogels for TEM sample preparation tended to shrink without internal support from silica template. The shrinkage of

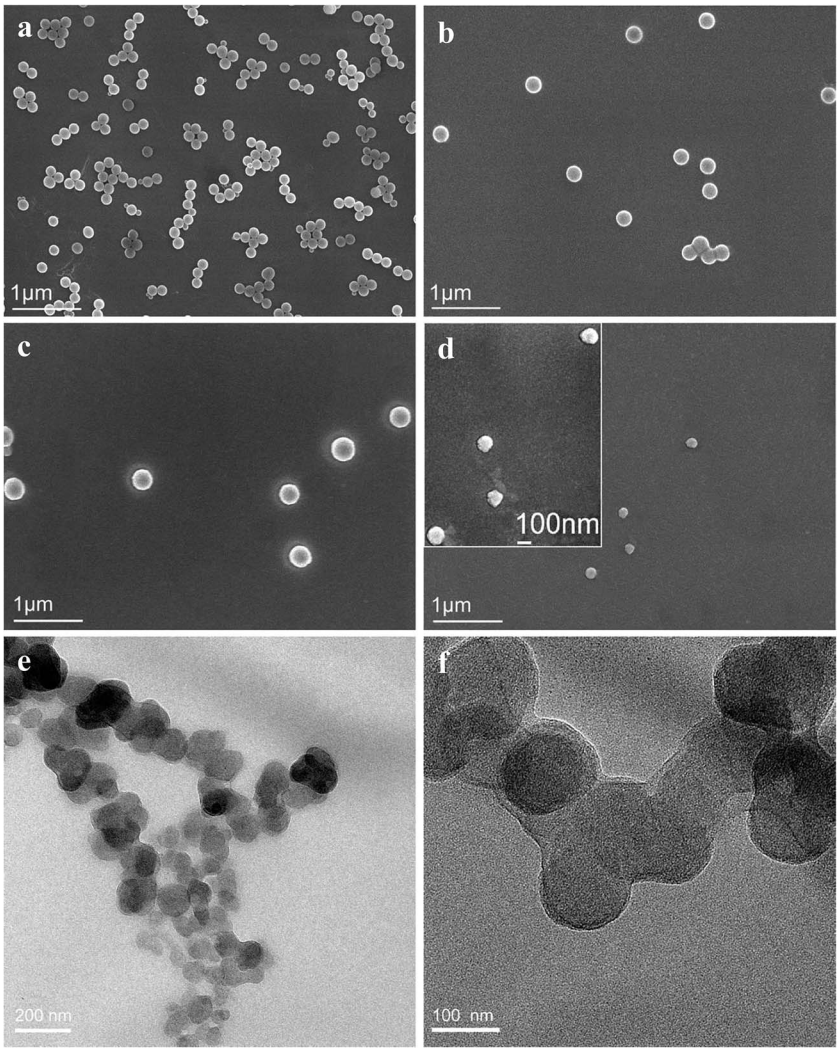

Fig. 4 Morphology of PLGA/CS nanogels (NG1). SEM images of (a) SiO_2 nanoparticles, (b) SiO_2-*g*-PLGA nanoparticles (NP1-*g*-PLGA), PLGA/CS nanogels (NG1) (c) before and (d) after core removal. (e) TEM images of PLGA/CS nanogels (NG1) at (e) low and (f) high magnification.

Open Access Article. Published on 07 March 2017. Downloaded on 2/2/2026 8:09:38 AM.
This article is licensed under a Creative Commons Attribution-NonCommercial 3.0 Unported Licence.

polymer-based spheres after dissolving the inner templates was also reported previously.[33]

TEM observation also showed that the PLGA/CS nanogels were spherical in shape, with a uniform particle size of about 100 nm (Fig. 4e and f), which was in good agreement with the SEM result. However, we failed to observe a hollow structure, which could be attributed to the great volume contraction of the swollen hollow PLGA/CS nanogels with thick shell (Part 3.3.2 and 3.3.3) upon evaporation of water during TEM sample preparation.[34]

3.3.2. Hollow structure of PLGA/CS nanogels. Micromorphology observation had indicated a spherical shape of PLGA/CS nanogels in dried state. In combination with electron microscopy, the geometric characteristics of nanogels in aqueous solutions were studied by determining their ratios of radius of gyration (mean-square radius; R_g) to hydrodynamic radius (R_h), R_g/R_h, derived from static light scattering (SLS) and dynamic light scattering (DLS) experiments, respectively.[35]

R_g/R_h is very sensitive to the particle morphology. Generally, the R_g/R_h values for spheres, vesicles with thin wall, and vesicles with wall thickness of about 1/3 their outer radius are 0.77, 1.0, and 0.86, respectively.[36,37] The DLS and SLS results for NG1 at 25 °C and pH 7.4 are shown in Fig. 5. DLS curve of PLGA/CS nanogels with R_h = 189.3 nm was presented in Fig. 5a. The R_g value was obtained from the partial Zimm plot of $KC/R_{vv}(q)$ *versus* q^2 by angle-dependent SLS measurements (Fig. 5b).[38] The R_g/R_h ratio of *ca.* 0.83 was essentially identical to the theoretical value (0.86), which indicated a hollow spherical shape of the nanogels with thick shell. The thick shell of the hollow PLGA/CS nanogels was in accordance with the wall thickness of about 90 nm displayed in Fig. 6b.

3.3.3. Fine size control of nanogels by silica templates. Typical size distribution profiles of nanogels before and after the removal of SiO_2 template were depicted in Fig. 6. Unimodal distribution patterns were found for all of the PLGA/CS nanogels. PLGA/CS nanogels with the average particle size of 365 nm (NG1), 315 nm (NG2) and 244 nm (NG3) were obtained using corresponding SiO_2 templates with the average size of 190 nm (NP1), 125 nm (NP2) and 78 nm (NP3), respectively. As shown in Fig. 6a, before and after silica template removal, there was almost no obvious difference in nanogel size and distribution, which might be ascribed to that the binding effect of the grafted PLGA to the silica core was sharply weakened along the radially outward direction, and removal of SiO_2 had little impact on the whole crosslinked network. It was worthwhile to mention that PLGA/CS nanogels after lyophilization could be homogeneously redispersed in water, and the size distribution profiles were similar to those of original ones before lyophilization, which was very favorable for application in drug delivery.

The nanogel size increased with silica template size. Using diameter of the nanogel and silica template as an outer diameter ($D_{nanogel}$) and inner diameter (D_{silica}) respectively, the nanogel had a wall thickness equal to half of the difference between $D_{nanogel}$ and D_{silica}. As shown in Fig. 6b, the wall thickness calculated was about 90 nm. There was not obvious difference in the wall thickness among NG1, NG2 and NG3. The

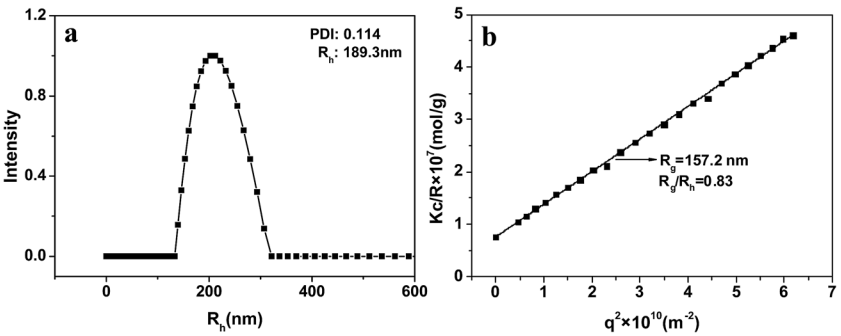

Fig. 5 Angle-dependent DLS (a) and SLS (b) data for PLGA/CS nanogels (NG1) in water at 25 °C.

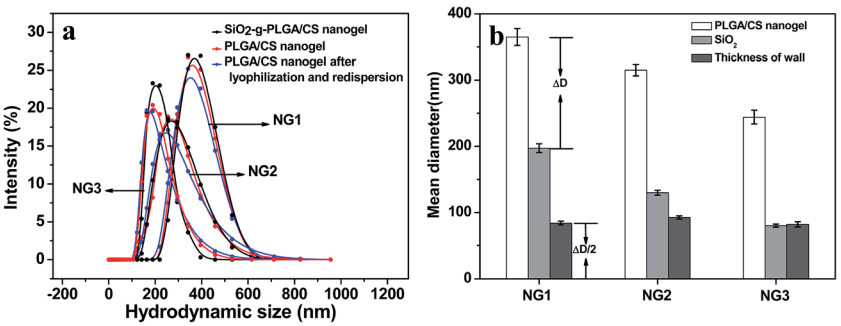

Fig. 6 (a) Hydrodynamic diameter distribution of PLGA/CS nanogels (NG1, NG2 and NG3) before and after SiO_2 template removal. (b) Theoretical value of thickness of nanogel wall in water calculated by size of SiO_2 and nanogels.

 This journal is © The Royal Society of Chemistry 2017

Open Access Article. Published on 07 March 2017. Downloaded on 2/2/2026 8:09:38 AM.
This article is licensed under a Creative Commons Attribution-NonCommercial 3.0 Unported Licence.

nanogel size could be estimated from the following formula: $D_{nanogel} = D_{silica} + \Delta D$ (polymer wall: ~180 nm). Therefore, the nanogel size could be effectively and accurately controlled by simply changing the silica template size. Similarly, it was reported that the size of the poly(*N*-isopropylacrylamide)-*co*-acrylic acid hydrogel cages could be controlled by using silica template core of varied size and different amount of monomers.[39] Xing *et al.*[40] also reported that the size and shape of the nanogel were controlled by SiO_2 template.

3.4. pH responsiveness, drug loading and release of PLGA/CS nanogels

3.4.1. pH responsiveness of PLGA/CS nanogels. Considering PLGA and CS were both weak polyelectrolytes, in order to investigate the pH-dependent behavior of PLGA/CS nanogels, the mean hydrodynamic diameter and zeta potential in various environments were obtained using DLS and electrophoretic light scattering, as shown in Fig. 7.

As expected, the hydrodynamic diameter of nanogel was found to vary with pH values of medium. The size of nanogels reached the minimum in the pH range of 4 to 6.5, and became significantly larger under both high and low pH conditions. Meanwhile, the zeta potential showed a monotonous decrease from positive values to negative ones in the pH range of 3.0 to 9.5. The size variation of the hydrodynamic diameter was governed by the internal osmotic pressure due to the mobile counter-ions contained within the nanogel containing pH-responsive groups, which balance the internal electrostatic repulsion.[41] In the case of low pH and high pH, the dominant charges in the nanogels were protonated amino groups ($-NH_3^+$) from CS and dissociated carboxylic groups ($-COO^-$) from PLGA, respectively. The electrostatic repulsion between these ionized groups induced swelling of nanogels. When the pH of medium was in range of pK_a of PLGA (4.4)[11] and pK_a of CS (6.3),[42] both PLGA and CS were partly ionized, and they could form compact interpolyelectrolyte complexes by electrostatic interaction. Therefore, the size of nanogels reduced to a minimum. Dai *et al.*[23] also found the electrostatic bonding of –COOH of PLGA and $-NH_2$ of CS was strongest at pH = 4–5.

3.4.2. pH-Dependent MTX encapsulation and *in vitro* release. Because of the large cavity inside the hollow nanogel and the network structure of polyelectrolyte shell, the PLGA/CS nanogels were expected to have promising application as drug carriers. Here, mitoxantrone (MTX), a water-soluble antineoplastic agent, was used as model drug to study the loading and release behavior of PLGA/CS nanogels. The hydrodynamic diameter and zeta potential of PLGA/CS nanogels (NG1) at different pH were presented in Fig. 8.

Compared with blank PLGA/CS nanogels, the zeta potential after MTX loading was significantly increased, as shown in Fig. 8a. Meanwhile, the size of drug loaded PLGA/CS nanogels reduced obviously at a pH ranging from 5 to 9 (Fig. 8b). As previously reported, MTX bore positive charge because of positively charged nitrogen atoms from the lateral chains of the drug,[43] while the PLGA/CS nanogels were negatively charged at a pH 5 to 9.3. The increasing zeta potential and decreasing size of PLGA/CS nanogels after MTX loading could be ascribed to electrostatic interaction between nanogels and MTX, as schematically illustrated in Fig. 8c. Chen *et al.*[44] also found the size of poly(acrylic acid) nanogels decreased after loading bovine serum albumin (BSA) with opposite charge.

Fig. 8d demonstrated the influence of pH value on the MTX loading capacity. The loading content increased greatly with the increase of pH value, from 14.3% of loading capacity at pH 4 to 43.6% at pH 9. The pH dependence of MTX loading could be ascribed to two factors. On one hand, there existed electrostatic interaction between MTX and nanogels, since MTX was positively charged at pH under 9.3,[45] while PLGA/CS nanogels showed negative charge at a pH ranging from 5 to 9.3 (Fig. 7b and 8a). It was reported that the percentages of positively charged MTX decreased from 100 to 58.5%, when pH value increased from 4.0 to 7.4.[45] However, the zeta potential of PLGA/CS nanogels decreased greatly from 8.79 to −14.2 mV when pH increased from 4.0 to 9.0. The strength of this interaction between nanogels and MTX predominantly depended on the charge of –COOH groups, which became stronger with increasing pH values due to the higher degree ionization of –COOH groups of PLGA chains, resulting in increased loading content. On the other hand, the size increased with increasing pH, facilitating the drug penetration and diffusion. At the pH value of 4, it was surprising that positively charged PLGA/CS nanogels (Fig. 7b and 8a) were capable of loading positive MTX, which might be ascribed to the hydrogen bonding between nanogels and MTX, and the cavity inside the hollow

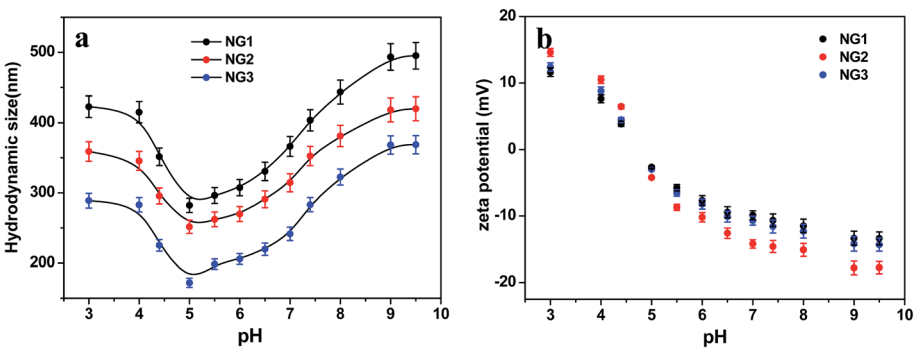

Fig. 7 pH responsiveness of PLGA/CS nanogels. Variation of (a) size and (b) zeta potential of PLGA/CS nanogels at different pH values.

Open Access Article. Published on 07 March 2017. Downloaded on 2/2/2026 8:09:38 AM.
This article is licensed under a Creative Commons Attribution-NonCommercial 3.0 Unported Licence.

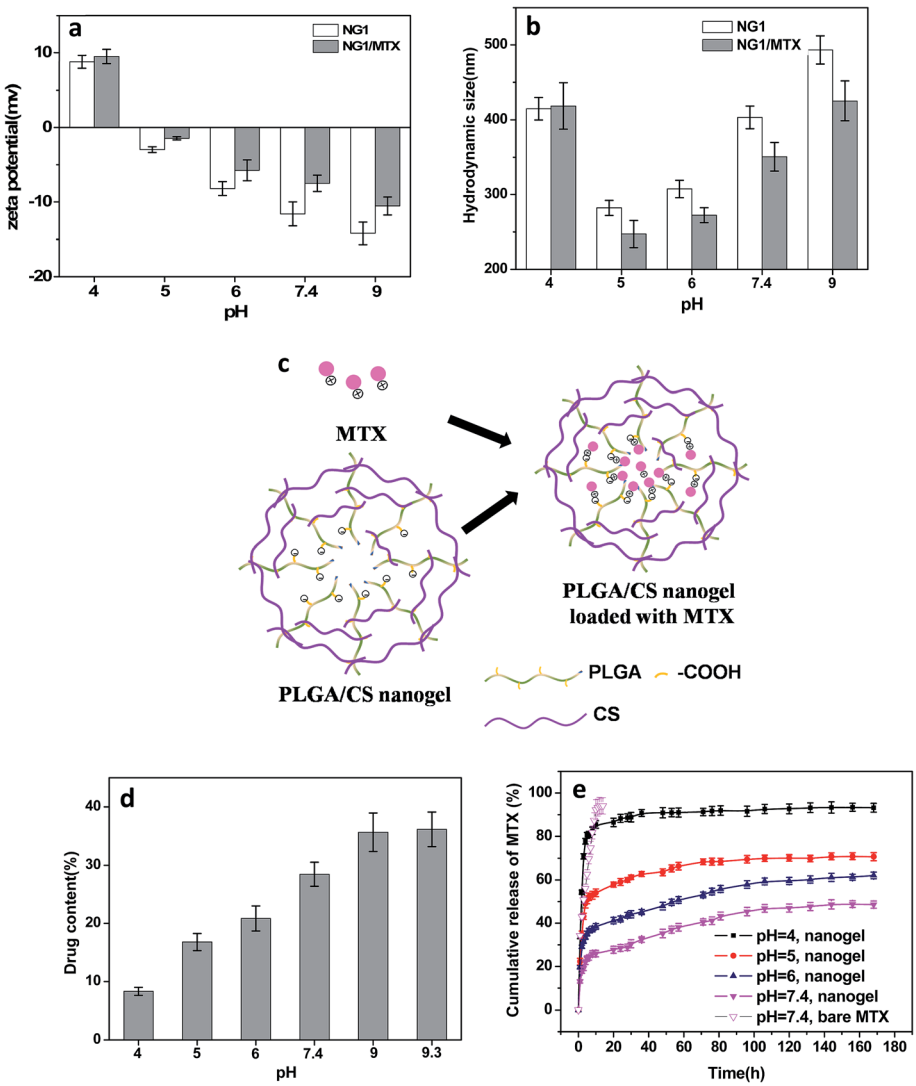

Fig. 8 pH-Dependent MTX encapsulation and *in vitro* release. (a) Zeta potential and (b) hydrodynamic size of MTX-loaded PLGA/CS nanogels (NG1) at different pH values. (c) Schematic representation of MTX loaded in PLGA/CS nanogels. (d) MTX loading content as a function of pH value. (e) Release profiles of MTX from PLGA/CS nanogels (NG1) at different pH values.

nanogels. Recently, Toh *et al.*[46] also reported the successful loading of MTX into nanodiamonds with positive charge *via* physical adsorption.

The release behavior of MTX from PLGA/CS nanogels (NG1) as a function of pH were shown in Fig. 8e. For comparison, the release profile of bare MTX was also depicted. The bare MTX in pH 7.4 buffer released rapidly. The initial burst release was severe with a release amount of 75.3% within 9 h. Compared with bare MTX, the release of MTX from PLGA/CS nanogels was obviously delayed. The pH value greatly affected the release profile of MTX loaded PLGA/CS nanogels. Quick release still could be observed within the first 10 h at pH 4, followed by a release balance with a cumulative release of 93.2%. This was due to the electrostatic repulsion between positively charged hydrogels and MTX bearing the same charge. Moreover, remarkable swelling at pH 4 was conducive to drug penetration and release. The cumulative release of MTX was only 35% within a week under the physiological conditions (pH 7.4). However, by adjusting the solution pH to acidity, MTX was released in significant amounts from the drug-loaded hydrogels into the external environment, *i.e.*, 47.9% at pH 6 and 62.1% at pH 5 within a week. Actually, the hydrodynamic diameter of PLGA/CS nanogels increased with increasing pH value in the pH range of 5 to 7.4, which might accelerate MTX penetration and release. Nevertheless, drug release was greatly restricted at higher pH value, which could be ascribed to the dominant effect of electrostatic interaction. As discussed above, the electrostatic interaction between PLGA/CS nanogels and MTX was stronger at higher pH value, greatly restricting drug release. Similarly, Ma *et al.* had reported a pH-responsive release of MTX by varying the electrostatic interaction between negatively charged silicate and positively charged MTX under designed pH 4–7.4 in PBS solution.[45] Duan *et al.* also found rapid MTX release at low-pH environment from supramolecular vesicles self-assembled by host–guest inclusion complex, they ascribed this phenomenon to pH triggered vesicles collapse.[47]

 This journal is © The Royal Society of Chemistry 2017

Open Access Article. Published on 07 March 2017. Downloaded on 2/2/2026 8:09:38 AM.
This article is licensed under a Creative Commons Attribution-NonCommercial 3.0 Unported Licence.

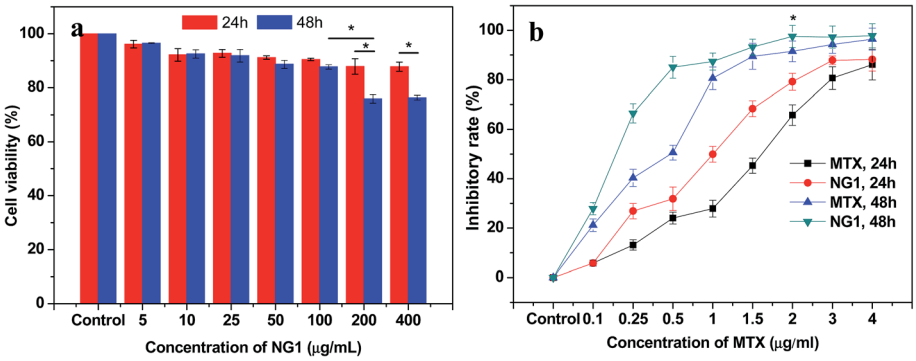

Fig. 9 Cytotoxicity of PLGA/CS nanogels and anticancer effect of MTX-loaded PLGA/CS nanogels. (a) L929 cell viability after 24 and 48 h of treatment by PLGA/CS nanogels (NG1) at different concentrations ($n = 3$, $^*p < 0.05$). (b) Inhibitory rate of MTX and MTX-loaded PLGA/CS nanogels (NG1) against human gastric carcinoma SGC7901 cells. The MTX concentration ranged from 0.1 to 4 μg mL^{-1} ($n = 3$, $^*p < 0.05$).

All the above evidences illustrated the electrostatic interaction between PLGA/CS nanogels and MTX was the key driving force for drug loading and release. The MTX release from PLGA/CS nanogels showed a good response to physiologically relevant pH (pH 4.0–7.4). It was well known the microenvironment of tumor cells was acidic for both intracellular and extracellular compartments, the rapid release of MTX from MTX-loaded hydrogels could be triggered by the acidic microenvironment of tumor cells, which was extremely significant for specific targeted therapy.[45,47]

Although the pH-responsive drug delivery systems for MTX have been developed based on mesoporous silica nanoparticles,[45] nanodiamond,[46] supramolecular vesicles self-assembled by pillar[6]arene and ferrocene derivative,[47] *etc.* However, the unsatisfactory biodegradability of inorganic nanoparticles, and instability of supramolecular vesicles in physiological environment have been limiting their effective applications. Comparatively, PLGA/CS nanogels have been found to be more desirable pH-responsive carriers for MTX delivery, because of their various advantages, such as biodegradability, stability in physiological environment, high loading and controllable release.

3.5. Cytotoxicity of PLGA/CS nanogels and anticancer effect of MTX-loaded PLGA/CS nanogels

The cytotoxicity of PLGA/CS nanogels was evaluated in fibroblast L929 cells *via* an MTT assay. As shown in Fig. 9a, the cell cytotoxicity of L929 cells treated with blank PLGA/CS nanogels (NG1) was above 90% when the final concentration of the nanogels was less than 100 μg mL^{-1}. Besides, there was no significant difference in cellular viability at 24 h and 48 h. All these indicated that the blank PLGA/CS nanogels showed a negligible cytotoxicity at a concentration of no more than 100 μg mL^{-1}. When the concentration was further increased to 200 and 400 μg mL^{-1}, the cell viability was decreased to approximately 80% at 48 h, showing the cell viability had a dose and time dependence. The result suggested that the NG was cytocompatible and suitable for future biological applications.[48]

The potential applications in the biomedical fields were assessed by investigating the cancer cell inhibition of MTX-loaded PLGA/CS nanogels against the human gastric carcinoma SGC7901 cells using the MTT assay. As revealed by Fig. 9b, both MTX and MTX loaded PLGA/CS nanogels (NG1) exhibited obvious inhibition effect on the cancer cells. And the inhibitory rate was higher upon 48 h incubation than that at 24 h incubation on the condition of the same concentration of MTX (≤2 μg mL^{-1}). SGC7901 cells treated with the MTX-loaded PLGA/CS nanogels showed the substantially higher inhibitory rate than those treated with the same concentration MTX, which might be attributed to the efficient delivery of the drug into the cells in the absence of PLGA/CS nanogels.

3.6. Cellular uptake of PLGA/CS nanogels

The cellular uptake of PLGA/CS nanogels was evaluated with fluorescence microscopy and flow cytometry. Fluorescence microscopy was used to visualize the internalization of RB and RB-loaded PLGA/CS nanogels (NG1) into the gastric carcinoma SGC7901 cells. Fig. 10a–c shows that in the SGC7901 cells, the nucleus exhibited a red layer of fluorescence after 4 h of culture with the RB. The fluorescent signal in the SGC7901 cells treated with the RB-loaded nanogels (Fig. 10a′–c′) was much stronger than in cells treated with the RB alone. It was reported that CS decorated on the nanoparticle surface facilitates cellular internalization *via* the unspecified sugar receptors on the cell membrane.[49] PLGA/CS nanogels adsorbed onto the surface of the cell membrane could be internalized by an endocytotic means, which permitted the delivery of high concentration of drug into cell.[50]

The cellular uptake of the PLGA/CS nanogels by SGC7901 cells was further demonstrated by flow cytometer analysis after 24 h of incubation with RB, RB-loaded PLGA/CS nanogels. As shown in Fig. 10d, the fluorescence intensity of cells incubated with RB-loaded PLGA/CS nanogels (NG1) was significantly higher than that of cells incubated with the RB in the test concentration range, suggesting that the internalization ability of the RB-loaded nanogels for the cancer cells are greater than that of the bare RB.

These results suggested that the PLGA/CS nanogels could efficiently enhance the cellular uptake by SGC7901 cells, which would contribute to increase the therapy efficacy for tumor.[51]

Open Access Article. Published on 07 March 2017. Downloaded on 2/2/2026 8:09:38 AM.
This article is licensed under a Creative Commons Attribution-NonCommercial 3.0 Unported Licence.

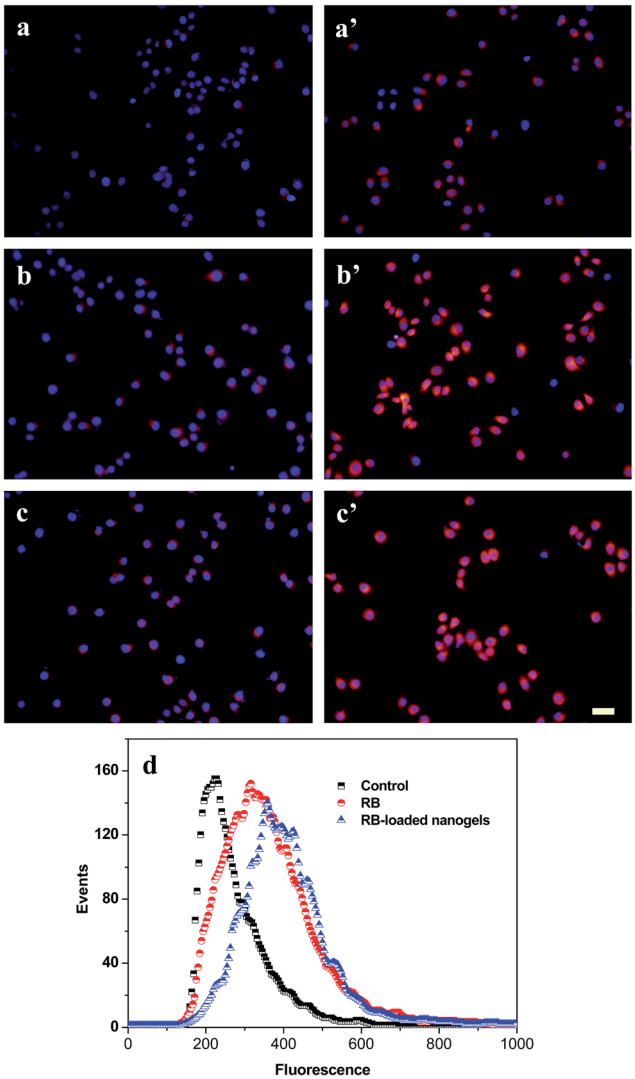

Fig. 10 Cellular uptake of the PLGA/CS nanogels. Fluorescence micrographs of human gastric carcinoma SGC7901 cells incubated with RB (a–c) and RB-loaded PLGA/CS nanogels (NG1) (a′–c′) at the RB concentration of 10 (a and a′), 50 (b and b′) and 100 μg mL^{-1} (c and c′). Blue fluorescence shows nuclear staining with DAPI and red fluorescence shows the location of RB encapsulated in the nanogels. Scale bar 50 μm. (d) Flow cytometry analyses of the SGC7901 cells after 4 h of incubation with RB and RB-loaded PLGA/CS nanogels (NG1). The RB concentration was set at 50 μg mL^{-1}.

4. Conclusions

In this study, we have synthesized a series of novel hollow PLGA/CS nanogel by combining templating approach with a "grafting from" method and intermacromolecules crosslinking technique. This strategy was showed to be versatile, simple, and suitable for precise control of the nanogel size. The resultant PLGA/CS nanogels exhibited pH-dependent response, which was elucidated according to the variation of size of nanogels and zeta potential at different pH values. The loading capacity of MTX increased greatly from 14.3 to 43.6% when the pH value increased from 4 to 9. The release behavior of MTX from the PLGA/CS hydrogels could also be controlled by changing solution pH values. Rapid release could be observed in acidic condition with significant cumulative drug release amounts from the MTX-loaded hydrogels, *i.e.*, 47.9% at pH 6, 62.1% at pH 5, and 93.2% at pH 4 within a week. MTT assays indicated that the PLGA/CS nanogels showed negligible cytotoxicity and were highly compatible with mouse fibroblast L929 cells. MTX loaded PLGA/CS nanogels exhibited higher inhibition effect on the cancer cells than free MTX. Fluorescence microscopy and flow cytometer analysis demonstrated that PLGA/CS nanogels could be efficiently delivered into the SGC7901 cells.

Therefore, the excellent pH responsiveness, quick release of MTX at acidic pH environment, efficient drug delivery and improved cytotoxicity to the human gastric carcinoma SGC7901 cells enabled the MTX-loaded PLGA/CS hydrogels to be used as a promising and effective carrier for controlled drug release and anti-tumour therapies.

Acknowledgements

The work was supported by the National Natural Science Foundation of China (no. 51473090 and 51373094), the Natural Science Foundation of Shanghai City (no. 14ZR1414600) and the Science and Technology Commission of Shanghai Municipality (No. 15JC1490400). Mr Yuliang Chu from Instrumental Analysis and Research Centre (Shanghai University) is acknowledged for their help in SEM measurement.

References

1 A. N. Koo, H. J. Lee, S. E. Kim, J. H. Chang, C. Park, C. Kim, J. H. Park and S. C. Lee, *Chem. Commun.*, 2008, 6570–6572.
2 W. Q. Shen, Y. L. Chang, G. Y. Liu, H. F. Wang, A. N. Cao and Z. S. An, *Macromolecules*, 2011, **44**, 2524–2530.
3 H. A. Abd El-Rehim, E. A. Hegazy, A. A. Hamed and A. E. Swilem, *Eur. Polym. J.*, 2013, **49**, 601–612.
4 T. G. Van Thienen, B. Lucas, F. M. Flesch, C. F. van Nostrum, J. Demeester and S. C. De Smedt, *Macromolecules*, 2005, **38**, 8503–8511.
5 N. Singh and L. A. Lyon, *Chem. Mater.*, 2007, **19**, 719–726.
6 M. Motornov, H. Royter, R. Lupitskyy, Y. Roiter and S. Minko, *Langmuir*, 2011, **27**, 15305–15311.
7 F. Maggi, S. Ciccarelli, M. Diociaiuti, S. Casciardi and G. Masci, *Biomacromolecules*, 2011, **12**, 3499–3507.
8 V. Dudnik, G. B. Sukhorukov, I. L. Radtchenko and H. Mohwald, *Macromolecules*, 2001, **34**, 2329–2334.
9 S. Argentiere, L. Blasi, G. Morello and G. Gigli, *J. Phys. Chem. C*, 2011, **115**, 16347–16353.
10 T. Zhou, C. F. Xiao, J. Fan, S. M. Chen, J. Shen, W. T. Wua and S. Q. Zhou, *Acta Biomater.*, 2013, **9**, 4546–4557.
11 C. Li, *Adv. Drug Delivery Rev.*, 2002, **54**, 695–713.
12 Y. C. Chang and C. W. Frank, *Langmuir*, 1996, **12**, 5824–5829.
13 W. Stöber, A. Fink and E. Bohn, *J. Colloid Interface Sci.*, 1968, **26**, 62–69.
14 M. Idelson and E. R. Blout, *J. Am. Chem. Soc.*, 1958, **80**, 4631–4634.

This journal is © The Royal Society of Chemistry 2017

Open Access Article. Published on 07 March 2017. Downloaded on 2/2/2026 8:09:38 AM.
This article is licensed under a Creative Commons Attribution-NonCommercial 3.0 Unported Licence.

15 I. Irurzun, J. J. Bou, G. Perez-Camero, C. Abad, A. Campos and S. Munoz-Guerra, *Macromol. Chem. Phys.*, 2001, **202**, 3253–3256.
16 C. Wu and S. Q. Zhou, *Phys. Rev. Lett.*, 1996, **77**, 3053–3055.
17 K. Nozawa, H. Gailhanou, L. Raison, P. Panizza, H. Ushiki, E. Sellier, J. P. Delville and M. H. Delville, *Langmuir*, 2005, **21**, 1516–1523.
18 M. Kar, P. S. Vijayakumar, B. L. V. Prasad and S. S. Gupta, *Langmuir*, 2010, **26**, 5772–5781.
19 F. Audouin, M. Fox, R. Larragy, P. Clarke, J. Huang, B. O'Connor and A. Heise, *Macromolecules*, 2012, **45**, 6127–6135.
20 G. Subramanian, R. P. Hjelm, T. J. Deming, G. S. Smith, Y. Li and C. R. Safinya, *J. Am. Chem. Soc.*, 2000, **122**, 26–34.
21 E. S. Cantu, S. T. Selcuk, J. Qiu, Z. Zhou and P. S. Russo, *Langmuir*, 2010, **26**, 15604–15613.
22 S. F. Yan, W. Ling and E. L. Zhou, *J. Cryst. Growth*, 2004, **17**, 226–233.
23 Z. Z. Dai, J. B. Yin, S. F. Yan, T. Cao, J. Ma and X. S. Chen, *Polym. Int.*, 2007, **56**, 1122–1127.
24 B. Cao, S. F. Yan, L. Cui, X. S. Chen and Y. T. Xie, *Macromol. Biosci.*, 2011, **11**, 427–434.
25 J. L. Hong, H. W. Choi, K. J. Kim and S. C. Lee, *Chem. Mater.*, 2006, **18**, 5111–5118.
26 J. Zheng, X. J. Tian, Y. F. Sun, D. R. Lu and W. L. Yang, *Int. J. Pharm.*, 2013, **450**, 296–303.
27 J. Fang, Y. Zhang, S. Yan, Z. Liu, S. He, L. Cui and J. Yin, *Acta Biomater.*, 2014, **10**, 276–288.
28 S. Yan, K. Zhang, Z. Liu, X. Zhang, L. Gan, B. Cao, X. Chen, L. Cui and J. Yin, *J. Mater. Chem. B*, 2013, **1**, 1541–1551.
29 S. Park, J. Park, H. Kim, M. J. Song and H. Suh, *Biomaterials*, 2002, **23**, 1205–1212.
30 M. J. B. Wissink, R. Beernink, J. S. Pieper, A. A. Poot, G. H. M. Engbers, T. Beugeling, W. G. Van-Aken and J. Feijen, *Biomaterials*, 2001, **22**, 151–163.
31 Z. J. Song, J. B. Yin, K. Luo, Y. Z. Zheng, Y. Yang, Q. Li, S. F. Yan and X. S. Chen, *Macromol. Biosci.*, 2009, **9**, 268–278.
32 J. Xu, S. Strandman, J. X. Zhu, J. Barralet and M. Cerruti, *Biomaterials*, 2015, **37**, 395–404.
33 C. Wang, C. He, Z. Tong, X. Liu, B. Ren and F. Zeng, *Int. J. Pharm.*, 2006, **308**, 160–167.
34 L. J. Shi and C. Berkland, *Macromolecules*, 2007, **40**, 4635–4643.
35 E. Kokufuta, K. Ogawa, R. Doi, R. Kikuchi and R. S. Farinato, *J. Phys. Chem. B*, 2007, **111**, 8634–8640.
36 W. M. Wan, X. L. Sun and C. Y. Pan, *Macromolecules*, 2009, **42**, 4950–4952.
37 H. J. Dou, M. Jiang, H. S. Peng, D. Y. Chen and Y. Hong, *Angew. Chem., Int. Ed.*, 2003, **42**, 1516–1519.
38 C. Wu and S. Q. Zhou, *Phys. Rev. Lett.*, 1996, **77**, 3053–3055.
39 J. X. Gu, F. Xia, Y. Wu, X. Z. Qu, Z. Z. Yang and L. Jiang, *J. Controlled Release*, 2007, **117**, 396–402.
40 Z. M. Xing, C. L. Wang, J. Yan, L. Zhang, L. Li and L. S. Zha, *Soft Matter*, 2011, **7**, 7992–7997.
41 W. T. Wu, J. Shen, P. Banerjee and S. Q. Zhou, *Biomaterials*, 2010, **31**, 8371–8381.
42 C. K. S. Pillai, W. Paul and C. P. Sharma, *Prog. Polym. Sci.*, 2009, **34**, 641–678.
43 M. Enache and E. Volanschi, *J. Pharm. Sci.*, 2011, **100**, 558–565.
44 Y. Chen, X. Zheng, H. Qian, Z. Mao, D. Ding and X. Jiang, *ACS Appl. Mater. Interfaces*, 2010, **2**, 3532–3538.
45 Y. H. Ma, L. Zhou, H. Q. Zheng, L. Xing, C. G. Li, J. H. Cui and S. N. Che, *J. Mater. Chem.*, 2011, **21**, 9483–9486.
46 T. B. Toh, D. K. Lee, W. Hou, L. N. Abdullah, J. Nguyen, D. Ho and E. K. H. Chow, *Mol. Pharmaceutics*, 2014, **11**, 2683–2691.
47 Q. P. Duan, Y. Cao, Y. Li, X. Y. Hu, T. X. Xiao, C. Lin, Y. Pan and L. Y. Wang, *J. Am. Chem. Soc.*, 2013, **135**, 10542–10549.
48 D. C. Che, X. X. Zhu, H. Z. Wang, Y. R. Duan, Q. H. Zhang and Y. G. Li, *J. Colloid Interface Sci.*, 2016, **463**, 1–7.
49 P. H. Weigel and J. H. Yik, *Biochim. Biophys. Acta*, 2002, **1572**, 341–363.
50 Y. T. Wang, S. S. Xu, W. F. Xiong, Y. Q. Pei, B. Li and Y. J. Chen, *Colloids Surf., B*, 2016, **146**, 107–113.
51 P. F. Liu, H. Yu, Y. Sun, M. J. Zhu and Y. R. Duan, *Biomaterials*, 2012, **33**, 4403–4412.